J Mater Sci (2007) 42:3825–3830
DOI 10.1007/s10853-006-0460-6

Effects of different particle sizes on electrochemical performance of spinel $LiMn_2O_4$ cathode materials

Ting-Feng Yi · Xin-Guo Hu · Chang-Song Dai · Kun Gao

Received: 8 February 2006 / Accepted: 16 May 2006 / Published online: 12 February 2007

Abstract Spinel $LiMn_2O_4$ were prepared by adipic acid-assisted sol–gel method at 800 °C, and the cathode materials with different particle sizes were obtained through ball milling. The effects of different particle sizes on electrochemical performance of $LiMn_2O_4$ sample were investigated by X-ray diffraction (XRD), galvanostatic charge–discharge test, cyclic voltammetry (CV), and electrochemical impedance spectroscopy (EIS), respectively. XRD data exhibits that all samples exhibit the same pure spinel phase; EIS and CV indicate that $LiMn_2O_4$ samples with smaller particle size have higher charge transfer resistance and oxidation potential than that of other samples corresponding to the extraction of Li^+ ions, respectively; galvanostatic charge–discharge test shows that the particle size has significant effects on the electrochemical performance of spinel $LiMn_2O_4$ cathode materials.

Introduction

Lithium ion rechargeable batteries are well regarded as a new promising power source for both portable electronic devices and zero emission vehicles (ZEV) due to their longer cycle life and higher energy density than other rechargeable battery systems. Currently there are mainly two types of cathode materials for lithium ion batteries. One is the layered $LiMO_2$ (M = Ni, Co, Mn) and the other is the spinel $LiMn_2O_4$ series. Spinel type lithium manganese oxide is one of the most attractive materials for use as a positive electrode for lithium ion batteries because of its high capacity, low cost, and low toxicity [1–7]. In spite of these advantages, $LiMn_2O_4$ has the problem of severe capacity fading during charge–discharge cycles, which makes it unsuitable for commercial performances. This problem has been discussed based on the following factors: manganese dissolution [8], electrolyte decomposition at high potentials [9], Jahn–Teller distortion at the deeply discharged state [10], and lattice instability [11]. There are also other factors that influence the battery performance, i.e., particle size and surface morphology. However, it is difficult to control such factors precisely using a conventional solid-state reaction method that requires long and repeated heat-treatment process. Such difficulties are expected to be solved by employing soft chemistry methods. In order to overcome the shortcomings of the solid-state reaction and improve the performance of spinel $LiMn_2O_4$ in batteries, sol–gel method was used in this paper. The sol–gel method gives spinel $LiMn_2O_4$ with a fine particle size, a narrow size distribution, and uniform composition, which leads to high electrochemical performance, so it has been widely used to prepare positive electrode materials of lithium ion batteries. It is well known that particle size is an important factor to judge the practicability of materials, because it not only relates to volume specific capacity of batteries but relates to electrochemical performance of batteries. The effects of particle size on the packing of cathode materials consisting of $LiMn_2O_4$ have been reported [12], but the electrochemical performance of spinel

T.-F. Yi (✉) · X.-G. Hu · C.-S. Dai · K. Gao
Department of Applied Chemistry, Harbin Institute of Technology, Harbin 150001, People's Republic of China
e-mail: tfyihit@hit.edu.cn

$LiMn_2O_4$ cathode materials with different particle sizes have not been investigated in detail. In this work, we synthesized a series of spinel $LiMn_2O_4$ cathode materials with different particle sizes using a sol–gel method, and the relationship between the particle size and electrochemical performance in lithium ion battery were examined.

Experimental

Preparation of $LiMn_2O_4$ cathode materials with different particle sizes

Spinel $LiMn_2O_4$ cathode material powder was synthesized by the sol–gel method using adipic acid as a chelating agent. The precursor was obtained as follows. First, stoichiometric amounts of reactants $Li(CH_3COO) \cdot 2H_2O$ (AR, 99%), and $Mn(CH_3COO)_2 \cdot 6H_2O$ (AR, 99%) were dissolved in distilled water to give a saturated solution with mild stirring. A saturated aqueous solution of adipic acid was then added at 1:1 molar ratios with the total metal ions. The pH of the mixed solution was maintained 6.5 by adding ammonium hydroxide solution. The solution was then heated at 80 °C with vigorous stirring to remove excess ammonia and water. The metal adipate precipitate so formed was dried in vacuum drying oven for 12 h at 110 °C. After drying, the precursors were decomposed at 350 °C for 5 h in air to eliminate organic contents. The decomposed powders were ground slightly and then calcined at 800 °C for 10 h in air, so the $LiMn_2O_4$ powders were obtained. The $LiMn_2O_4$ samples with different particle sizes were obtained by ball milling the $LiMn_2O_4$ powders above mentioned which were prepared at the same synthesis time and temperature. The ball milling was carried out in a ND-6 planetary ball milling machine (Nanjing, China) for different times of 200 rpm in air.

Characterization of $LiMn_2O_4$ cathode materials

Differential thermal analysis (DTA) and thermogravimetery (TG) measurements were performed in air from room temperature to 1,000 °C with a ZRY-2P thermal analysis system (Shanghai, China) under a scanning rate of 5 °C min^{-1}. Powder X-ray diffraction (XRD) was performed on Rigaku D/MAX-RC X-ray diffractometer with $CuK\alpha_1$ (45 kV 50 mA, step size = 0.02°, $10° < 2\theta < 90°$) monochromated radiation in order to identify the crystalline phase of the materials. Cyclic voltammetry (CV) was measured on an electrochemical workstation (CHI 430A) at a scan rate of 0.1 m V s^{-1} between 3.3 and 4.5 V (versus Li/Li^+). The EIS tests were carried out at room temperature using a Model 273 potentiostat (made by EG&G Princeton Applied Research), a 5210 phase-lock amplifier, a NEC Powermate ITX computer system, and EG&G M 398 EIS testing system in a range of 0.1 Hz–100 kHz. The $LiMn_2O_4$ electrodes were adopted as the work electrode; the counter electrode and reference electrode were Li foil. The results of the measurements were analyzed by using the EG&G EQUIVCRT software. Mastersizers laser diffraction particle size analyzer was used to analyze the particle size of ground $LiMn_2O_4$ samples.

Preparation of lithium ion batteries

For the preparation of cathode sheets, a slurry was formed by mixing the active material (85%), acetylene black (10%), and binder (5 wt% polyvinylidene fluoride, PVDF, dissolved in *N*-methyl-2-pyrrolidone, NMP). The mixed slurry was coated onto an aluminum current collector. The electrodes were dried under vacuum at 110 °C overnight and then punched and weighed. The batteries were assembled in a glove box under a dry and high purity argon atmosphere (99.999%). The complete coin cell comprises a cathode, a celgard 2300 (polypropylene) as the separator and a lithium foil anode. About 1 M $LiPF_6$ (battery grade) dissolved in a mixture of ethylene carbonate (EC, battery grade) and dimethyl carbonate (DMC, battery grade) (1:1 by volume) was used as the electrolyte. Charge–discharge performance of the cell was characterized galvanostatically on BTS 5 V/5 mA battery testing system (Shenzhen, China) at about C/5 charge–discharge rate between 3.3 and 4.5 V (versus Li/Li^+).

Results and discussion

TG–DTA analysis

Figure 1 shows the TG–DTA curves for the thermal decomposition of the precursor $LiMn_2O_4$.

Weight loss occurs in four temperature regions: 20–120, 120–300, 300–400, 400–1,000 °C. The little weight loss of the first region may be attributed to the superficial water loss due to the hygroscopic nature of the precursor complex. In the second region, the DTA curve shows two endothermic peaks at 138.1 and 232 °C, which are attributed to the loss of water of chemical bond water in the samples. In the third

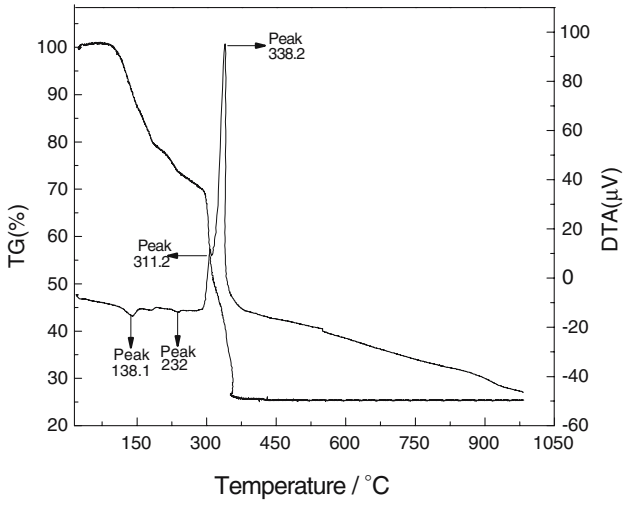

Fig. 1 The TG–DTA curves for the thermal decomposition of the precursor $LiMn_2O_4$

region, the two exothermic peaks observed at 311.2 and 338.2 °C are accompanied by noticeable weight lose in the TG curve. It is due to the decomposition of the inorganic and the organic constituents of the precursor followed by crystallization of $LiMn_2O_4$ phase. In the last region, the TG curve becomes flat and no sharp peaks can be observed in the DTA curve, indicating that no phase transformation occurs, and that any further heating only makes the structure of samples more crystalline.

Crystal structure analysis

The XRD patterns for $LiMn_2O_4$ samples with different particle sizes are shown in Fig. 2.

All samples are identified as a pure spinel phase with a space group *Fd3m* where Li^+ ions occupy the tetrahedral (8a) sites; Mn ions reside at the octahedral (16d) sites; and O^{2-} ions are located at (32e) sites. XRD analysis reveals that all $LiMn_2O_4$ with different particle sizes have the same XRD pattern, and no additional peaks for other second phases such as Mn_2O_3 are observed, indicating that the solid-state reaction has been completed at this condition. We calculated the lattice parameters of all samples from the diffraction data through the least square program method and found that all $LiMn_2O_4$ samples with different particle sizes had approximately equal lattice parameters value (8.2383 ± 0.004 Å).

Studies of charge–discharge

The relation between the specific discharge capacity, the cycle number and particle size is plotted in Fig. 3.

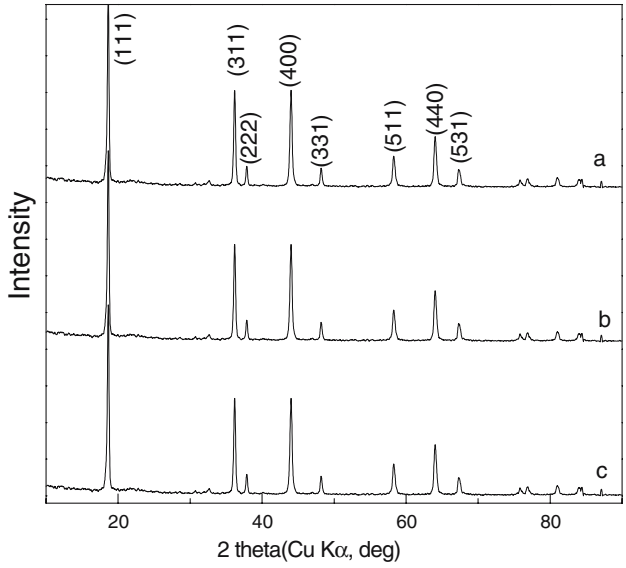

Fig. 2 XRD pattern of $LiMn_2O_4$ samples with different particle sizes (a) D_{50} = 4.2 μm; (b) D_{50} = 16.3 μm; (c) D_{50} = 40.7 μm (D_{50} means average particle size)

In the first cycle, it is found that the discharge capacities for the samples with D_{50} (D_{50} means average particles size) = 4.2, 16.3, 40.7 μm, are 129.5, 129.4 and 130.0 mAh g^{-1}, respectively. After 50 cycles, the samples (D_{50} = 16.3 μm) also exhibit the largest capacity, and their capacity retentions are 79.07, 91.65, and 86.53%, respectively. Based on this concept, the particle size of $LiMn_2O_4$ samples slightly affects the initial discharge capacity, but it is an important factor in affecting the cycle ability. The tap density of materials with big particle size can be improved, but

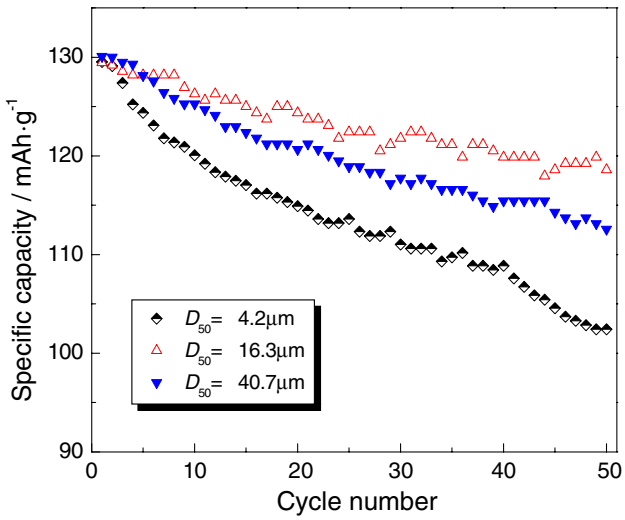

Fig. 3 Specific discharge capacity of $LiMn_2O_4$ with different particle sizes

the bigger of the particle size, the more serious of the distortion of crystal is in the course of charge–discharge, and the cycle performance of batteries declines. Smaller particle size is positive to improve cycle performance of batteries, though boundary of grain increases. For this reason, too small particle size increases the difficulty transferring electrons, and then polarization of batteries augments so that it goes against charge–discharge of batteries. Meanwhile, too small particle size can debase the tap density of materials so that the energy density of batteries is affected. Moreover, too small particle size increases the surface area of active materials, so the dissolution of Mn^{3+} become more serious, which leads that active component of materials decreases gradually, and the granules are difficult to contact each other which makes the capacity decrease [13]. At the same time, the deliquescent manganese deposits negative electrode, and the passivation layer is formed, so it reduces the conductance and blocks the transportation of electrons and ions [14, 15]. As a result, the cycle performance of battery decreases seriously as shown in Fig. 3 (D_{50} = 4.2 μm). Hence, optimization of particle size is an important determinant of the performance for lithium rechargeable batteries.

The Coulomb efficiency of $LiMn_2O_4$ samples with different particle sizes was also measured as shown in Fig. 4.

This efficiency is defined as the discharge capacity divided by the charge capacity in one charge–discharge cycle. In the first cycle, the efficiency of $LiMn_2O_4$ with D_{50} (D_{50} means average particles size) = 16.3, 31.2, 40.7 μm, are 94.1, 93.1, and 93.7%, respectively, indicating that a small fraction of lithium ions is incapable of intercalating back into the host structure. However, after cycling for two or three runs, the Coulomb efficiency is increased to a nearly constant value. However, the $LiMn_2O_4$ powder with D_{50} = 16.3 μm has the highest average value of Coulomb efficiency as shown in Fig. 4. The above result reveals that the $LiMn_2O_4$ sample with D_{50} = 16.3 μm exhibits the best electrochemical performance among three sieved powders. The reason is may be that the overall surface area of the cathode material is increased during charge–discharge cycle, and the cathode material consisting of small particles with large interface area can provide more lithium ions for diffusion which need only to travel a shorter path inside the particle than in large one, leading to the high ionic current. In addition, during the discharge process, small particles can provide more interfacial area for contact within the liquid electrolyte and hence can increase the opportunity for lithium ions to intercalate back into the host structure, thereby resulting in the high Coulomb efficiency.

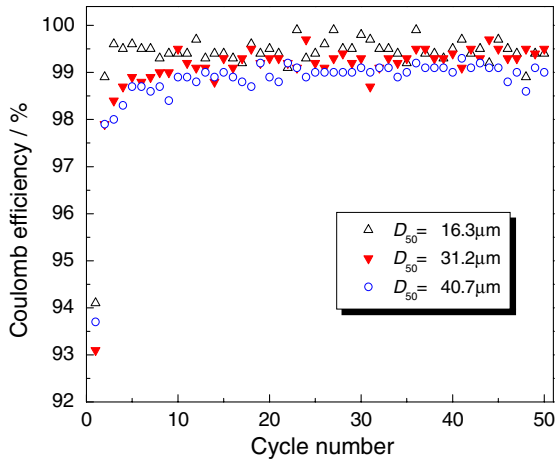

Fig. 4 Coulomb efficiency of $LiMn_2O_4$ samples with different particle sizes

Studies of electrochemical characteristics

To investigate further the effects of different particle sizes on the kinetics of the electrode processes, EIS result of $LiMn_2O_4$ samples after 30 cycles with different particle sizes at 100% discharge state (discharged to 3.3 V) is given in Fig. 5.

The EIS patterns displayed at Fig. 5 consist of two semicircles and a straight line. The obscure small semicircle appearing in the high-frequency region reflects the resistance (R_f) of migration of Li^+ ions through the surface films, and film capacitance (C_f) [16–18]. The middle-frequency capacitive loop is

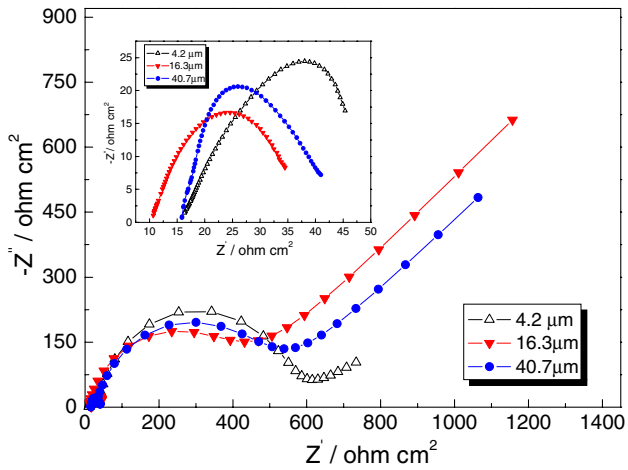

Fig. 5 Niquist plots for the $LiMn_2O_4$ samples with different particle sizes at 100% discharge state (discharged to 3.3 V) after 30 cycles

caused by charge transfer resistance (R_t) and interfacial capacitance (C_{dl}). The low-frequency straight line can be attributed to diffusion of Li^+ ions in the samples [19]. The diffusion rate of Li^+ in electrolyte solution is far greater than that of Li^+ in solid-state active material, so the resistance of charge transfer can be considered as the rate-determining step of the diffusion process of Li^+ during the charge–discharge of battery. The characteristics of these electrodes, represented by the equivalent circuit, are shown in Fig. 6, where R_S is the solution ohmic resistance of the electrode system, R_f and C_f are, respectively, the resistance and capacitance of a solid electrolyte interphase (SEI) film, and W is the Warburg impedance of solid-phase diffusion.

Fitted results from EIS are displayed in Table 1. It can be seen from Table 1 that the R_f values of different samples are almost constant, whereas R_t values vary greatly with different particle sizes. The minimum R_t values of the sample (16.3 μm) mean the lowest electrochemical polarization, and this leads to higher cycle performance. The largest R_t values indicate that the sample (4.2 μm) has largest electrochemical polarization, which results in their relatively lower cycle performance. The reason may be that the small-particle material has formed poor crystallinity or too many defects after several cycles because of the distortion of crystal in the course of charge–discharge corresponding to the capacity fading as shown in Fig. 3 (D_{50} = 4.2 μm). This often occurs when the smaller particle was prepared through ball milling, because the crystallite grains are not well maintained during the grinding.

In order to further investigate the extraction/intercalation behavior of Li^+ ions, cyclic voltammetry

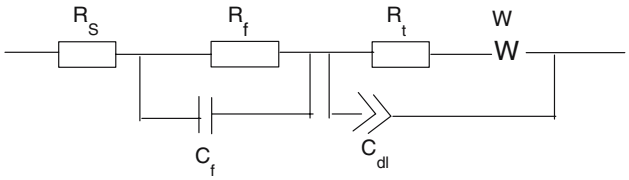

Fig. 6 Equivalent circuit used to analyze the EIS

Table 1 Some data of the samples with different particle sizes obtained by EIS fitting

	Sample (4.2 μm)	Sample (16.3 μm)	Sample (40.7 μm)
R_S (ohm cm^2)	13.92	10.10	18.87
R_f (ohm cm^2)	25.83	24.89	25.14
R_t (ohm cm^2)	497.9	385.7	452.3

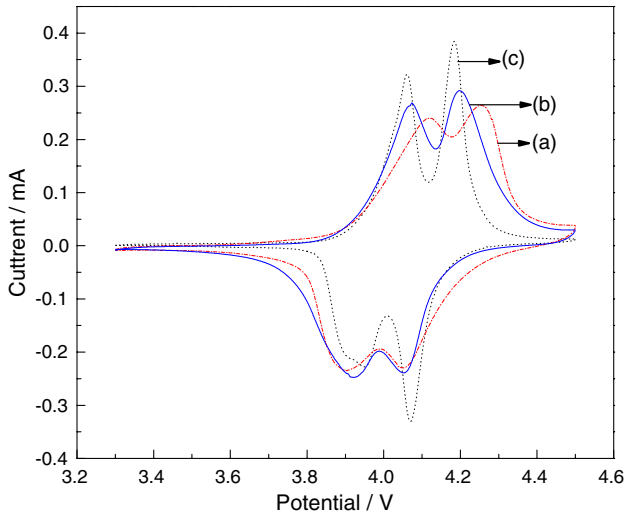

Fig. 7 Cyclic voltammetry of $LiMn_2O_4$ samples with different particle sizes (a) 4.2 μm; (b) 16.3 μm; and (c) 40.7 μm

analysis was performed. Figure 7 illustrates the cyclic voltammetry for $LiMn_2O_4$ samples with different particle sizes.

All specimens display two peaks indicating that the solid-state reaction has been completed, which represents the mixed phases and different intercalation stages of lithium ions [20]. However, during the oxidation procedure, it is found that the $LiMn_2O_4$ samples with D_{50} = 4.2 μm has higher oxidation potential than that of other samples corresponding to the extraction of Li^+ ions. Deintercalation of Li^+ ions at higher potential indicates that more driving force is necessary to impel the lithium ions from the host structure to the anode. This implies that there is higher the resistance of charge transfer existing in small particle $LiMn_2O_4$ than in large one. These results are in agreement with EIS test above. Therefore, it has an important significance by controlling appropriately particle size to improve the performance of materials.

Conclusions

A series of $LiMn_2O_4$ positive electrode materials with different particle sizes were prepared by adipic acid-assisted sol–gel method. All $LiMn_2O_4$ samples with different particle sizes exhibit good crystal structure. Particle size has significant effects on the electrochemical performance of $LiMn_2O_4$ positive electrode materials, and $LiMn_2O_4$ with D_{50} = 16.3 μm shows better capacity retention among these samples. The cathode materials with too big or small particle sizes arouse capacity fading, but the initial discharge capacity is

only slightly affected. The $LiMn_2O_4$ cathode materials with small particle size have higher Coulomb efficiency and bigger resistance of charge transfer than the large one. It is important to improve the performance of $LiMn_2O_4$ materials by controlling appropriately particle size.

Acknowledgements The authors gratefully acknowledge financial support from Harbin Institute of Technology. The authors also thank Dr. Ying Wang of Institute of Chemistry Chinese Academy of Sciences for his helpful discussion on the experimental techniques.

References

1. Fukutsuka T, Sakamoto K, Matsuo Y, Sugie Y, Abe T, Ogumi Z (2004) Electrochem Solid-State Lett 7:A481
2. Sun YC, Wang ZX, Huang XJ, Chen LQ (2004) J Power Sources 132:161
3. Tarascon M, Wang E, Shokoohi FK, Mckinnon WR, Colson S (1991) J Electrochem Soc 138:2859
4. Thackeray MM, Johnson PJ, Picciotto LA, Bruce PG, Goodenough PG (1984) Mater Res Bull 19:179
5. Xia Y, Zhou Y, Yoshio M (1997) J Electrochem Soc 144:2593
6. Pistoia G, Antonini A, Rosati R, Zane D (1996) Electrochim Acta 41:2863
7. Guyomard D, Tarascon JM (1992) J Electrochem Soc 139:937
8. Gadjov H, Gorova M, Kotzeva V, Avdeev G, Uzunova S, Kovacheva D (2004) J Power Sources 134:110
9. Aurbach D, Markovsky B, Shechter A, Ein-Eli Y, Cohen H (1996) J Electrochem Soc 143:3809
10. Matsuda K, Taniguchi I (2004) J Power Sources 132:156
11. Yamada A (1996) J. Solid State Chem 122:160
12. Vacassy R, Hofmann H, Papageorgious N, Gratzel M (1999) J Power Sources 81:621
13. Dziembaj R, Molenda M (2003) J Power Sources 119–121:121
14. Tarascon JM, Mckinnon WR, Coowar F, Bowmer TN, Amatucci G, Guyomard D (1994) J Electrochem Soc 141:1421
15. Wen SJ, Richardson TJ, Ma L, Striebel KA, Ross PNJR, Cairns EJ (1996) J Electrochem Soc 143:L136
16. Levi MD, Aurbach D (1997) J Phys Chem B 101:4630
17. Levi MD, Levi EA, Aurbach D (1997) J Electroanal Chem 421:89
18. Aurbach D, Levi MD, Levi EA (1998) J Electrochem Soc 145:3024
19. Wang GG, Wang JM, Mao WQ, Shao HB, Zhang JQ, Cao CN (2005) J Solid State Electrochem 9:524
20. Miura K, Yamada A, Tanaka M (1996) Electrochim Acta 41:249